ap

Asian Journal of Physics
Vol. 29, Nos 10-12 (2020) 835-852
Available on: www.asianjournalofphysics.in

Role of self-referenced interferometry in measuring the orbital angular momentum of optical vortices: A review

Praveen Kumar[1], Naveen K Nishchal[1] and Kehar Singh[2]

[1]*Department of Physics, Indian Institute of Technology Patna, Bihta, Patna-801 106, India*

[2]*Department of Applied Sciences, The NorthCap University, Gurugram- 122 017, India*

This article is dedicated to Prof FTS Yu for his significant contributions to Optics and Optical information Processing

Association of optical vortices with the orbital angular momentum of light provides a new understanding of various optical and physical phenomena. For widespread applications of vortex beams in diverse areas, different techniques for their efficient generation and detection have been investigated. Self-referenced interferometric techniques are often encountered to examine the phase singularity of optical vortices through intensity measurements. This paper reviews the recent progress in techniques for topological charge measurement of vortex beams emphasizing the role of self-referenced interferometry.

Keywords: Optical vortices, Vortex beam, Orbital angular momentum, Phase singularity, Interferometry.

1 Introduction

In nature, several physical phenomena of vortices exist which are studied in multiple areas of physics ranging from fluid dynamics, atmospheric physics, quantum physics to optics and photonics [1]. Vortices appear in fluid dynamics where the flow revolves around an axis, which give rise to common phenomena such as tornadoes and whirlpools. Because of the importance of these phenomena, the study of dislocations in an optical field has become a topic of intense study. The foundation for the study of wavefront dislocations was laid by the pioneering work of Nye and Berry [2]. Later, Coullet *et al* [3] investigated the manifestation of vortex in structured light field analogous to vortex flow in hydrodynamics and introduced the term optical vortices.

Wavefront dislocations can be observed in optical fields having strong spatial inhomogeneity. The typical singularity structure related to the gradient of phase that arises in a paraxial light beam with a helical phase profile is referred to as optical vortex (OV) [3]. The amplitude of light becomes zero at phase singularity which results in isolated dark intensity spots. The OV is formed from the twist of energy and electromagnetic momentum flow around the singular point. Optical vortex beams (VBs) have brought up many innovations, which have been summarized in several review articles and books [4-7].

Being scalar, phase singularity can exist independent of polarization. Incorporating vectorial nature of light brings further singularity in optical field associated with polarization [7,8]. At each point in the transverse plane of an optical field, the time-varying direction of electric field traces an ellipse. The parameters such as its ellipticity and the orientation of the major axis given by azimuth angle are used to characterize the state of polarization. Polarization singularities arise in a region of non-uniformly polarized elliptical

Corresponding author :
e-mail:nkn@iitp.ac.in (Naveen Kumar Nishchal)

or vector field where the parameters used to characterize the state of polarization becomes ambiguous. C-point polarization singularity occurs at a point of circular polarization in an elliptical field of spatially varying polarization states with non-zero ellipticity and gradually varying azimuth across the transverse plane. Another type of polarization singularity is V-point which occurs at a null intensity point in a vector field consisting of linear polarization states with spatially varying azimuth. The vortices in an optical field embedded with both phase and polarization singularity are referred to as vector vortices [9]. The general results of investigations on optical field singularities created a new topic in modern optics, which is known as singular optics [10]. Currently, many active investigations are undergoing on a variety of platforms. Review articles summarizing significant developments with the fundamental theories and applications of optical singularities have been reported [7,11,12].

The rest of the paper is organized as follows: Sections 2 and 3 describe the features of OVs such as their topological charge (TC) and orbital angular momentum (OAM), respectively. Different forms of VB and their various applications have been reviewed in sections 4 and 5, respectively. Sections 6 and 7 briefly summarize the common methods of generation and detection of VBs, respectively. In Section 8, the research progress in self-referenced interferometric techniques for determining TC of VBs is highlighted. Various configurations of self-referenced interferometry for interferogram formations have been discussed in Section 9. Methods for measuring the TC of vector-VBs have been reviewed in section 10. Finally, some conclusions are drawn in Section 11.

2 Optical vortex beam and its topological charge

Optical vortex beams are produced when the light with helical wavefront rotates like a corkscrew, around the phase singularity that lies along the propagation axis [13]. Laguerre-Gaussian (LG) modes have a helical phase profile and they hold optical vortex. The electric field amplitude of LG mode which propagates along z-direction can be expressed in terms of their local coordinates [14] as,

$$E(x, y; l) = \sqrt{\frac{2p!}{\pi(p+|l|)!}}\frac{1}{w(z)}\left[\frac{1\sqrt{2}}{w(z)}\right]^{|l|}\exp\left[\frac{-r^2}{w^2(z)}\right]L_p^{|l|}\left(\frac{2r^2}{w^2(z)}\right)\exp\left[\frac{k_0 r^2 z}{2(z^2+z_R^2)} - i\psi + il\phi\right] \tag{1}$$

where ϕ denotes the azimuth angle, $\phi = \tan^{-1}(y/x)$ and l is the azimuthal index also referred to as the TC. $w(z)$ is the $1/e$ radius of Gaussian term, which is given by $w(z) = w(0)\left[\frac{(z^2+z_R^2)}{z_R^2}\right]^{1/2}$. Here $w(0)$ denotes beam waist and Z_R is the Rayleigh range. $L_p^{|l|}$ is the associated Laguerre polynomial, p is the radial nodes in the intensity distribution, ψ is Gouy phase given by $\psi = (2p + |l| + 1)\tan^{-1}(z/z_R)$, and $r = \sqrt{x^2+y^2}$.

The field distribution at a short transmission distance z_0 denoted as $E'(x, y)$ can be calculated using the Fresnel diffraction [8],

$$E'(x, y) = \exp\frac{ikz_0}{i\lambda(z_0)}\iint_{\Sigma} E(x', y')\exp\left[i\frac{k_0}{2z_0}\{(x-x')^2 + (y-y')^2\}\right]dx'dy' \tag{2}$$

where λ denotes the wavelength of light and $k_0 = 2\pi/\lambda$. The integral limits correspond to the source area Σ and the coordinates x' and y' denote the variables of integration.

The singularity in phase arises at a region around which the phase changes by the signed integral multiple of 2π. The phase profile and the phase-front of a VB of TC = 1 are shown in Figs 1 (a) and (b), respectively. At the region of phase singularity, the phase is indeterminate and light amplitude is zero resulting in the doughnut-shaped intensity profile as shown in Fig 1 (c). TC is an important parameter which

specifies the order of singularity [13]. The magnitude of TC is equal to the number of the windings of the phase per revolution around the singular point. The direction in which phase increases gives the sign of TC. For an opposite sign of TC, the phase increases in the opposite direction around the singular point.

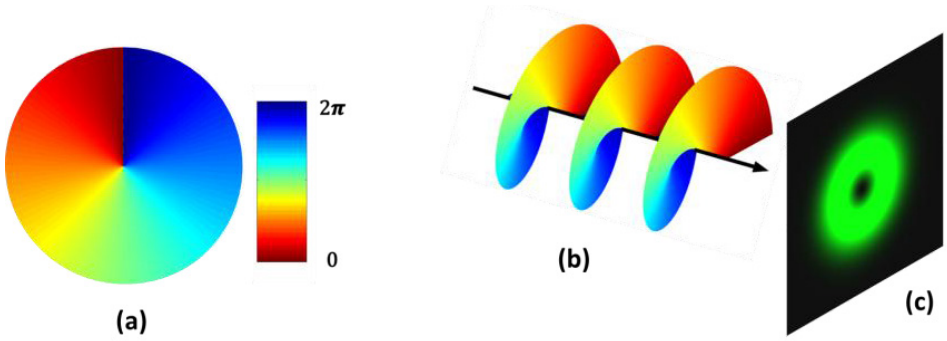

Fig 1. (a) Phase profile, (b) phase-front, and (c) intensity profile of a VB of TC = 1.

3 Orbital angular momentum of light

Light beam that carries OAM, is a donut-looking structured light form. It is characterized by an azimuthally twisted phase profile with a central intensity null. OAM modes are usually produced external to the laser cavity. Creation of OAM modes directly from a laser is difficult because nature can not differentiate between a clockwise and anticlockwise mode. Both these modes bear same propagation dynamics, same beam sizes, same wavefront curvature, and so on. For generating such symmetric modes, some form of symmetry breaking is required. It was first suggested by Poynting in 1909 that light may carry angular momentum [14]. In 1936, Beth demonstrated the rotation of a physical object (a quarter-waveplate suspended on a thread) with circularly polarized light and showed that angular momentum of light can result in measurable mechanical torque [14]. In a study by Allen *et al* in 1992, it was understood that the total angular momentum of light has both spin and an orbital component [14]. Spin angular momentum (SAM) is associated with polarization, whereas OAM is associated with the spatial mode of light. The process of conversion from SAM of light into OAM was demonstrated through the interaction of light with optically inhomogeneous and anisotropic matter [14]. Many review articles on the total angular momentum of light are available in literature [15-18].

It was realized that the light with azimuthal phase dependence carries well-defined OAM [15]. The azimuthal phase profile is mathematically represented by $\exp(il\phi)$, where ϕ is the azimuthal angle and l denotes the TC. Beam with such phase profile are embedded with optical vortices and carries OAM that depends on TC as $\pm lh/2\pi$ per photon, where h is the Planck's constant. Unlike polarization, which has two orthogonal states, TC associated with OAM may take any integer value. The combination of the concept of OAM with the idea of optical vortices created new possibilities in classical and quantum optics, which have expanded their functionality in diverse areas [18-20].

4 Forms of vortex beams

Earliest reported VB carrying OAM are the LG modes which have azimuthal phase dependence [6]. Besides TC, LG modes are also characterized by their radial index p. The intensity profile of LG modes comprises of $p + 1$ concentric bright rings for TC $\neq 0$. For a given beam waist, the radius of the ring depends on the TC. Many other OAM carrying light beams have been reported such as Bessel modes. Other OAM carrying light beams are Ince-Gauss modes, Hypergeometric-Gaussian modes etc [6]. For integral TC values, the wavefront of VBs forms perfect helices with a single screw-phase dislocation, on the beam axis. Non-

integer vortex structure has also been studied which has a complex-phase profile and comprises of many vortices at differing positions within the beam cross-section [7]. The size of the central dark hollow of the vortex has a strong dependence on its TC. For specific applications, such as optical trapping and manipulating the small particles, it is desired to provide a large TC and a small dark hollow simultaneously. For this purpose, the concept of the perfect optical vortices was introduced whose dark hollow radius does not depend on the TC [7].

Other than circular symmetric vortices, the existence of other forms of vortices of electromagnetic scalar wave fields has been reported such as elliptical vortices, hypergeometric vortex, and arbitrary shaped vortices [6,21]. Other kinds of VBs such as airy VB and asymmetric Bessel modes have also been reported [22,7]. These anomalous OVs result in versatile OAM distributions which are especially useful in areas such as optical tweezers and plasmonics. Phase singularities also occur when three, or more, plane-waves interfere [23]. For instance, OVs are found in speckle fields, where the random interference of waves creates points of phase singularity [7]. Methods for OV lattice formations have also been suggested [6,7].

5 Applications of vortex beams

Various physical phenomena based on OVs have been explored. The OAM of OVs unveils new understandings on light-matter interaction and connection between macroscopic optics and quantum effects.The transfer of SAM and OAM to the internal and external angular momentum of an atom has been investigated [16]. In 1995, He *et al* demonstrated the transfer of momentum from VB to particles resulting in their rotation [24]. The capability of OV to trap and manipulate the particles has expanded the applications of optical tweezers and different techniques of manipulating small particles using OV have been reported [14].

In optical imaging, light with a helical phase has led to improved sensitivity or limits of resolution [25]. Fürhapter *et al* utilized spiral wavefront of VBs in optical interferometry to override a basic problem that was to distinguish elevations and depressions in a phase sample [25]. In light microscopy, methods for edge contrast enhancement of phase samples have been demonstrated using the spiral phase. Tamburini *et al* proposed the use of OVs to achieve super-diffraction-limit imaging for applications in applied optics and astronomy [6]. Optical VBs have been found useful in astronomical applications. For instance, Swartzlander *et al* used the dark core of an OV to examine a weak background signal hidden in the glare of a bright light source for detection of an astronomical object and introduced an OV coronagraph for imaging of astronomical objects [14]. Investigations have been carried out for diffraction of singular beams to study the influence of aberrations on the intensity distribution for their effective applications [26,27].

Mair *et al* observed entanglement of OAM between down-converted pairs of photons and demonstrated the quantum nature of OAM [14]. Beams carrying OAM has brought significant innovations in the field of quantum optics which has been summarized in Ref [28]. Interferometric methods to measure orbital and spin or the total angular momentum of a single photon have been reported [28]. Quantum-controlled logic gates using OAM qubits have also been reported and investigations on entanglement evolution of a quantum OV state propagating through coupled lossless waveguides have been carried out [28,29]. LG modes have also led to innovations in quantum phenomena such as electromagnetically induced transparency [30].

SAM of light is associated with the polarization which can be described in the two-dimensional (2D) basis of right and left circular polarization, whereas OAM has an infinite number of eigenstates, corresponding to different TC values. Therefore, in principle, the number of bits the OAM of a single photon can represent is unlimited. This makes OAM a promising parameter for encoding classical or quantum information [28]. Recent advances in optical communications using OAM have been presented in Ref [31].

Optical cryptographic techniques have been invented to protect information from unauthorized users utilizing different features of light [32]. Unbounded OAM states have great advantages in classical and

quantum cryptographic schemes. It is believed that security schemes based on laws of quantum mechanics can detect intruders trying to access the information [33]. In the quantum key distribution (QKD) protocol, identical secret keys are established at two remote locations to perform a secure transfer of information. Initial experiments on QKD used 2D quantum systems (qubits). It was proposed that OAM of a photon could be used to achieve a higher-dimensional system for quantum cryptography which results in higher information capacity and increased noise tolerance level at a given security level [34]. Classical information security schemes based on OAM of light have been developed to achieve a high-security holographic encryption system [35]. In one of the approaches, information encoded holograms were designed which correctly decode visual information only when illuminated with light with a specific order of OAM [36]. These systems appear promising for anti-counterfeiting applications.

OVs have applications in other areas such as optical metrology. Techniques for displacement or angular rotation measurements have been proposed that makes use of phase singularities carried by VBs [6]. Lavery *et al* analyzed the OAM of the light scattered from a spinning object and observed a frequency shift proportional to the product of the rotation frequency of the object and the OAM which can be used for the remote detection of rotating bodies [6]. OVs play an important role in the study of various phenomena. The phenomenon of vortex solitons in a nonlinear medium has been reported [14]. It was also demonstrated that an LG mode may undergo second-harmonic generation and the resulting frequency-doubled light is of a higher-order mode [19]. Allen *et al* showed that an atom moving in a light beam with OAM experiences an azimuthal shift in the resonant frequency in addition to the usual axial Doppler and recoil shifts [16]. Novel applications and innovations in fundamental theories brought by OVs have made it an extensive growing research field [5-7,10,11].

6 Generation of vortex beams

There has always been an effort to generate OVs in an efficient and controlled way owing to various applications. Laser beams with dislocations of different orders can be experimentally generated using diffractive holograms consisting of fork-shaped gratings or spiral Fresnel zone plates [14]. Spiral phase plates or vortex phase masks were also used to convert laser beam into a helical-wavefront beam [4,5]. VBs with non-integer TC can be also generated from a spiral phase plate with a non-integer phase step. Techniques have been developed to generate VBs directly from lasers [6].

Off-late, programmable electro-optic devices such as spatial light modulators (SLM) and digital micro-mirror devices (DMD) have been used in the generation of structured light beams due to the convenience and flexibility offered by these devices [19]. SLMs are capable of phase-only modulation of light. Desired 2D phase profile distributions can be modulated into the light by simply displaying the holograms onto the SLM. Through appropriate holograms, different forms of VBs can be generated such as LG modes, Bessel modes or Perfect VBs. These features have made SLMs a useful device for generating VBs of different orders. Methods of VB generation with tunable wavelength and chirality have also been reported [6]. Recent progress in techniques for VB generation has been summarized in Refs [19,37].

7 Measuring orbital angular momentum of optical vortex

The OAM associated with OV is vital information for the study of various physical phenomena and applications. Various intensity measurement-based techniques have been investigated to study the spatial structure of the phase, which is responsible for the different modes of OAM. Determining TC of VBs is a convenient way to measure the order of singularity and the amount of OAM carried by beams. Therefore, the development of efficient TC measurement techniques has become an area of extensive research. These methods can be categorized into interferometric and non-interferometric techniques.

7.1 Non-interferometric methods

In a pioneering work conducted by Beijersbergen *et al* in 1993, the interconversion between LG and HG modes was demonstrated using astigmatic elements which operate as mode converter [38]. In the astigmatic transform of VB, TC is indicated in the resulting intensity patterns of 2D optical lattices. For TC measurement, based on this principle, various optical systems were employed such as cylindrical lens [39], quadratic phase [40], twisting phase [41], cross-phase [42], and tilted lens [43]. In a comparative study, astigmatic transform with a cylindrical lens was found suitable for determining the TC of VB [44].

Another approach for measuring OAM is mode separation, which can be done in multiple ways. Using the geometrical phase transform, the VB is converted into a plane wave with a transverse phase gradient which produces a spot in the observation plane at different lateral positions depending on its TC [45]. Techniques based on this approach have been extended to measure the OAM spectrum of light and for sorting the OAM modes. Spiral transform was introduced to improve this technique to separate OAM modes with superior resolution while maintaining unity efficiency [46]. A mode transformer to decode the OAM was developed comprising of custom refractive optical elements which convert OAM states into transverse momentum states [47]. In literature, many other optical arrangements and phase masks have been employed to transform the VB into geometrical patterns of intensity which could reveal their TC [48-50].

Techniques based on specific features of light such as diffraction have been extensively investigated for probing OVs. It was observed that the VBs get diffracted from slits or apertures to produce exotic intensity pattern which exhibits their phase characteristics and is influenced by their TCs [51]. Therefore, to carry out the TC measurement, diffraction characteristics of VBs were examined employing various apertures such as triangular-apertures [52], diamond-shaped apertures [53], circular aperture [54], sectorial screen [55], annular aperture [56], and annular grating [57]. For TC determination other techniques have also been explored which are based on Fourier transformation [58], rotational Doppler effect [59], time mapping approach [60], and using a single point detector [61]. Methods with the capability to measure fractional OAM of light have also been reported [62].

7.2 Interferometric methods

Interferometric methods are the most common way to study the various properties of an optical field. It is one of the earliest methods to study the features of light beams with helical wavefront [63]. To observe the phase singularity and measure the OAM carried out by VB common way is to obtain interference with a reference beam [3-5]. Formation of fringe patterns is an outcome of the phase profiles of reference and the VB and therefore TC can be determined by interference fringe analysis [5,64]. In off-axis interference of VB with a planar wavefront beam, fringe pattern in the interferogram consists of bifurcation at the region of wavefront dislocation where the morphology of the bifurcation reveals its TC. Such fringe structure is similar to a fork-shaped pattern consisting of a handle and tines. The magnitude of TC is determined by counting the number of tines.

The in-line interference of a VB with a reference beam with spherical wavefront results in a fringe pattern that consists of spiral stripes around a singular point. Here, the number of spirals gives the TC of VB. In another configuration for measuring TC, interferogram consisting of petal-shaped fringe patterns can be obtained [65]. However, it was observed that an additional stand-alone reference beam may not be always available for interference which led to the development of self-referenced interferometric techniques. In this approach, input VB is made to interfere with its own amplitude or wavefront split copy to produce a well-defined fringe pattern, which can reveal its TC. These techniques allow a more intuitive way for TC determination using simpler implementation and hence are often used in the study of OVs and its applications.

In other approaches, diffracted orders of VBs are made to interfere to produce fork or spiral fringe pattern [66-68]. Methods based on a multipoint interferometer were found useful in measuring the OAM of

light from astronomical sources [69]. This approach was further used for quantitatively measuring the OAM of the photons [70]. Interferometric methods have also been employed to measure the spin and total angular momentum of even single photon [71].

8 Role of self-referenced interferometry in measuring TC of vortex beams

Recent developments in various configurations of self-referenced interferometric techniques for determining the TC of VBs have been summarized in this section. In this approach, input VB and its amplitude split copy, referred to as 'replicated beam' are made to interfere using certain optical arrangements such that the interferogram reveals TC. This split-beam method has been implemented since the early endeavors while investigating the helical nature of wavefront [72-74]. Since then this approach has been utilized in various applications of VBs for detection and diagnosis of the singularity order. Different optical configurations have been investigated to split the beam of interest and recombine them with sufficient modifications so that interference pattern becomes simpler to analyze for measuring TC [75-77].

In one of the configurations, sufficient misalignment between the interfering VBs were introduced to produce straight fringes and then in the transverse plane the beams were laterally displaced so that their singularities fall in relatively uniform areas where the spatial phase variation is small [78]. The interferogram consists of defects in the fringe pattern at each singularity position. At these dislocations, the fringe pattern has fork-shaped structures, which are analyzed to determine their TC. Different types of interferometers have been proposed with an ability to incorporate lateral displacement between interfering VBs such as Mach-Zehnder interferometer (MZI), lateral shear interferometer, wedge plate-based interferometer, and Sagnac interferometer [78,79]. The approach works even when the interfering beams have multiple numbers of singularities. However, the interference pattern gradually becomes complicated with too much singularity.

Further development was made in this configuration in which the tilt between the VBs and its replicated beam is incorporated in a controlled way along with the lateral displacement [80]. When the direction of applied tilt and lateral displacement become orthogonal the conjoined fork-shaped fringe pattern is formed. This type of fringe structure has an advantage in the unambiguous determination of TC. This is because the interferograms for VBs with opposite helicity are not simply mirror-images of each other unlike the previous configuration. The fork-structures in the interferogram are either connected by their tines or handles, depending on the sign of TC and the number of tines at their forks gives the magnitude of TC. Formation of such fringe patterns has been demonstrated using MZI and other shearing interferometers such as wedged optical flat [80-82].

While TC determination of VB, spiral-shaped fringe patterns are preferred over fork-shaped pattern in some cases, especially for high-order TCs. Therefore, attempts were made to produce a spiral-shaped fringe pattern through self-referenced interferometry. In one of the approaches, the amplitude split copy of input beam is clipped by a small aperture and then converted to a spherical beam using a lens which interferes with the original VB to form spiral-shaped fringe pattern [83]. Another way to obtain spiral fringes is by using an improved Fizeau interferometer where a test VB is incident on a flat-concave mirror at an oblique angle [84]. Optical elements of fixed structure used as interferometers are simpler to use but the quality of interferogram reduces for VB with high order TC.

The concept of lateral displacement was further utilized to produce a spiral-shaped fringe pattern with better visual inspection [85]. In this configuration, curvature difference was introduced between the interfering beams along with the lateral displacement. Based on the split-beam approach, desired interference field can be obtained using MZI by introducing a convex lens in one of its arms. Through analyzing the spiral interferogram, both sign and magnitude of TCs can be determined even of different orders. This method can also be used to measure fractional orders of TC.

In many configurations of self-referenced interferometry, lateral displacement is introduced between the interfering beams, which prevent their complete overlapping at the recoding plane of the interferogram [80]. As the TC of VB increases, the fringe structure at each dislocation becomes more complex and after a certain value of TC they tend to mix because of large vortex size. These factors make the interferogram difficult to interpret for high order measurements of TC and for other forms of VBs such as LG beams which have radial modes. Therefore, most of these techniques have been demonstrated for determining the TC only up to a few orders.

Another form of self-referenced interferometric approach has been reported where the test VB interferes with its mirror image (having opposite helicity). The in-line interference results in petal or spiral-shaped fringe pattern, depending on the curvature difference between the interfering beams [86]. The magnitude of TC can be determined by counting the number of petals or spirals. The helicity direction of VB is reversed on reflection, this phenomenon is utilized to obtain the interference between VB and its conjugate copy through various optical configurations such as using a bi-prism or MZI consisting of a dove prism [87,88]. A similar technique was reported which demonstrated the measurement of the fractional TC [89]. It was shown that the petal-shaped pattern can be utilized to study the interference properties of LG beams with non-zero radial modes. Using this approach, high-order TC (up to TC ~ 90) was measured by counting the number of petals in fringe pattern [90]. However, the sign of the TC could not be determined using this technique and as a solution a modified version was suggested incorporating two improved MZIs with dove prisms [91]. In this case, the input beam copy is transmitted through a spiral phase plate before directing into the second MZI. The sign of the TC is determined by comparing the number of petals in the interferograms of both MZIs.

Recently, a new technique for determining high-order TC of LG beams has been demonstrated by combining the concept of lateral displacement and phase conjugation [92]. This technique can be used to determine both sign and magnitude of TC carried by high-order LG beams. In this case, the input VB interferes with its own conjugate copy at a small angle. In addition, one of the interfering beams is displaced laterally to overlap with the other at the plane of interferogram recording. The optical set-up uses an MZI with a right-angle prism. Interferograms are produced with better visibility which consist of a fork-shaped fringe pattern. The number of tines in the fork-shaped pattern reveals the magnitude of TC and its sign is determined by the orientation of fork structure, which gets inverted with the inversion in helicity of the incoming VB.

9 Formation of interferograms in self-referenced interference of vortex beams

As discussed in previous sections, commonly used interferograms which reveal the TC of VB through visual analysis are a fork and spiral-shaped fringe patterns. In this section, the formation of these interferograms through different self-referenced interferometric configurations is discussed. In this study,

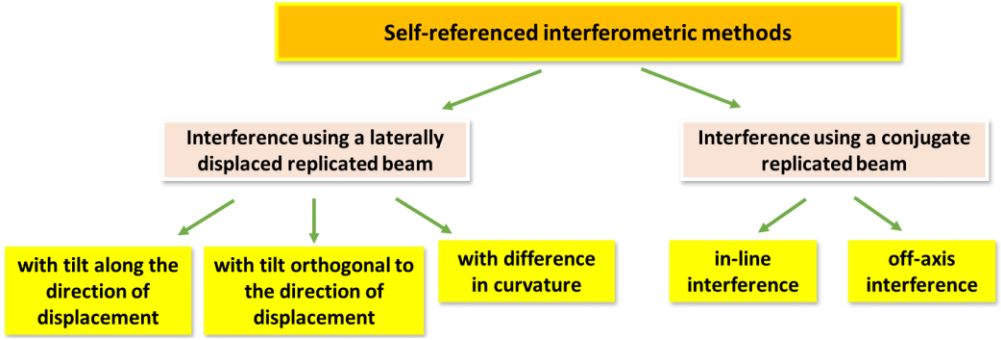

Fig 2. Flowchart of different configurations of self-referenced interferometric methods for TC measurement of VBs.

we consider interference between the VB and its modified replicated beam. For convenience, they have been referred to as beams 1 and 2 with electric field amplitudes E_1' and E_2', respectively. The electric field amplitude of beam 1 is obtained while substituting $l = l_1$ in Eq (2), hence $E_1' = E'(x, y; l_1)$. Based on the modifications incorporated in the replicated copy (beam 2), the interferometric configurations have been categorized into two types. In the first type, the interfering VBs are laterally displaced and have same TCs, whereas in other type interfering beams completely overlap each other and TCs have opposite sign. These configurations have been discussed in sub-sections 9.1 and 9.2, respectively. A flowchart of various configurations of self-referenced interferometry has been illustrated in Fig 2. One of the simplest ways to realize these configurations is through a MZI set-up, as shown in Fig 3.

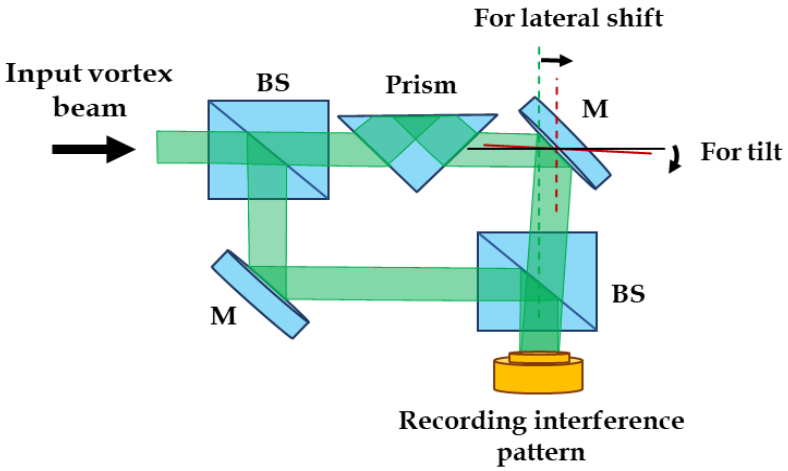

Fig 3. Schematic diagram of optical set-up for self-referenced interferometry. BS and M denote beam splitter and mirror, respectively. Lateral shift and tilt can be incorporated through a mirror. A right-angled prism is used when TC inversion of input VB is required.

9.1 Interference with a displaced replicated beam

Interference of a beam with its own laterally displaced replicated copy is a useful technique to examine the properties of a light beam. Interferograms consisting of a fork or spiral-shaped fringe patterns are formed when other interferometric arrangements such as tilt or curvature difference are introduced between the interfering beams along with the lateral displacement. Utilizing these parameters, three different configurations have been discussed in the subsequent sub-sections. To describe interferogram formation simulation has been carried out on MATLAB platform by considering a sample space that spans a finite physical area with side length of 4 mm along x and y directions. The value of wavelength used is 532 nm, radial index p is 0, beam waist $w(0)$ is 0.75 mm and the propagation distance is about 83 mm.

(*i*) *With tilt along the direction of displacement*

In this case, lateral displacement and tilt are simultaneously incorporated between interfering beams, which partially overlap each other in the recording plane [80]. The direction of tilt is incorporated along the direction of lateral displacement. The electric field amplitude of replicated VB consisting of helical phase and tilt function takes the form,

$$E_2 = E(x + \Delta x, y; l_2) \exp\left(ik_0((x + \Delta x)\tan\alpha + y\tan\beta)\right) \tag{3}$$

where E_2 denotes the resultant field and α and β are the tilt angles along x- and y-directions, respectively and l_2 is the TC. The term Δx is the lateral displacement in the beam wavefront incorporated to produce a small spatial shift in the transverse plane along the y-direction. The field distribution, E_2' at a propagation distance

z_0 is evaluated using the Fresnel diffraction solution as illustrated in Eq (2) and the intensity distribution of interference is given by $I = |E_1' + E_2'|^2$. The magnitude and sign of TCs remain equal ($l_2 = l_1$) and the parameters substituted in the replicated beam are $\Delta x = -1$ mm, $\alpha = -0.0025$ rad, and $\beta = 0$ rad.

The phase profiles of the interfering beams 1 and 2 are shown in Fig 4 (i) and the insets show the corresponding intensity distributions. The null intensity region indicates the presence of a singular point, which is at a shifted location in the VB copy (beam 2). The gradient in the phase profile illustrates the direction of tilt along the shift direction. The interferograms presented in same figures show the formation of the oppositely aligned fork-shaped fringe pattern. The Fig 4 (ii-a) corresponds to TC = 1, the interferogram shows that each disjoined fork structures have an extra discontinuous fringe starting from the dislocations. As the TC value increases the number of discontinuous fringes also increases as shown in Fig 4 (ii-b) for TC = 2. Therefore, the magnitude of TC can be determined by the relation $|l| = N - 1$, where N is the number of tines at the fork structure. The sign of TC is determined through the orientation of fork structure which inverts for a negative value of TC as illustrated in Fig 4 (ii-c). These types of fringe structures have been demonstrated using MZI, Michelson interferometer, and lateral shear interferometer [78-80].

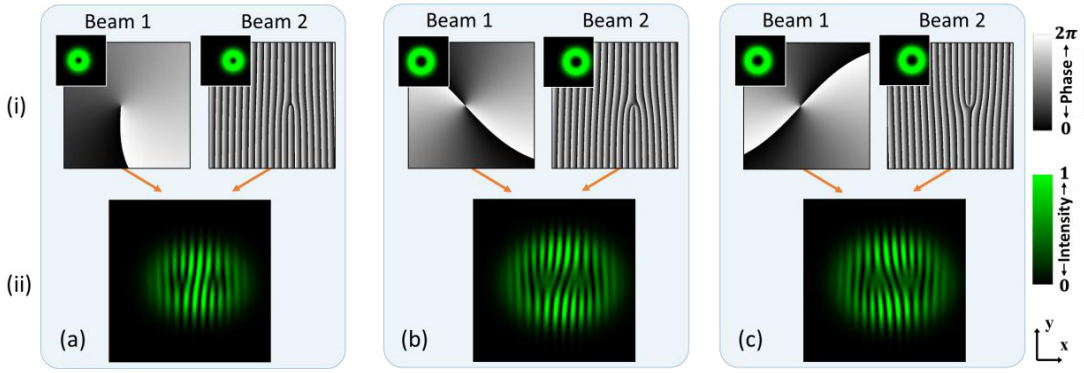

Fig 4. Formation of interferogram consisting of double fork-shaped patterns when VBs interfere with its replicated beam, which is laterally displaced and tilted along the same direction.

(*ii*) *With tilt orthogonal to the direction of displacement*

In this configuration, the interferograms are formed when tilt direction is introduced orthogonal to the direction of lateral displacement [80]. The modified replicated beam can be obtained from Eq (3) while substituting $\Delta x = -0.9$ mm, $\alpha = -0.0003$ rad, and $\beta = 0.0023$ rad. The TCs of interfering beams remain identical. A small amount of tilt is introduced along x-axis to compensate the displacement of the beam due to its tilt along y-direction. Formation of interferograms along with intensity and phase profile of the interfering beams have been shown in Fig 5. The intensity and phase profiles of the interfering beams are shown in Fig 5 (i). The direction of tilt is indicated by the gradient direction in the phase profile. The interferogram consists of conjoined fork-shaped structure. Figure 5 (ii-a) corresponds to TC = 1, where the forks share their tines which indicate positive (+) sign of TC, and the magnitude of TC is given by $|l| = N - 1$, where N is the number of tines. For TC = 2, the number of shared tines is 3 as shown in Fig 5 (ii-b) and for a negative (–) sign of TC, the forks are shared by their handle as shown in Fig 5 (ii-c).

In this case, the forks share either their tines or a handle depending on the sign of TC and therefore the fringe pattern obtained for positive and negative valued TCs as shown in columns (b) and (c) are not simply mirror images of each other. This feature allows unambiguous and simpler way of determining the sign and magnitude of TC carried by the VB. Formation of these fringe patterns have been demonstrated using interferometers such as MZI set-up and a wedged optical flat where the interfering beams are reflected from a piece of glass that has its two flat surfaces slightly wedged to each other [79-81].

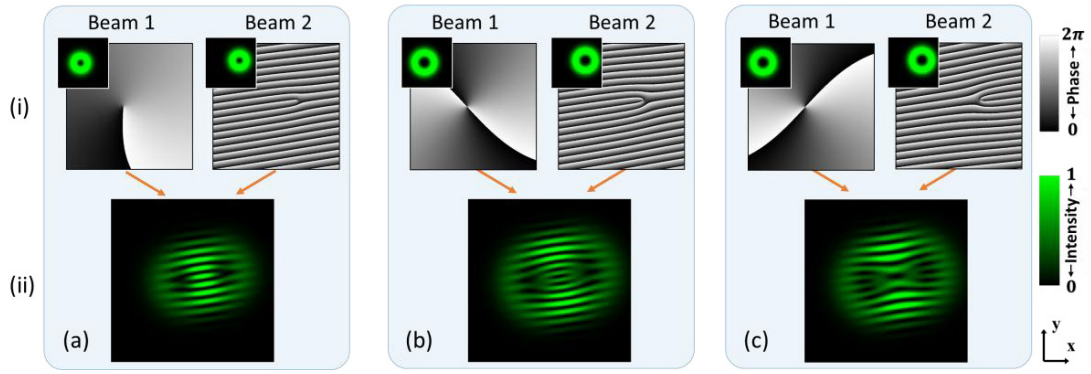

Fig 5. Formation of interferogram consisting of a conjoined fork-shaped pattern when VBs interfere with its replicated beam, which is laterally displaced and tilted along the orthogonal direction

(*iii*) *With difference in curvature*

In this interferometric arrangement, an appropriate amount of lateral displacement and curvature difference is simultaneously incorporated between the interfering VBs having the same sign and magnitude of TC [85]. The replicated beams obtained by duplicating the wavefront of the input VB is subjected to spatial shift in the transverse plane and change in the curvature. The electric field amplitude of this replicated VB takes the form,

$$E_2 = E(x + \Delta x, y; l_2) \exp\left\{-ik_0 \frac{(x + \Delta x)^2 + y^2}{2R}\right\} \tag{4}$$

This equation consists of helical phase functions and spherical phase function. E_2 is the resultant field amplitude and the corresponding TC is l_2. The field represented by Eq (4) when propagates a distance z_0, then the resultant field can be obtained using the Fresnel diffraction solution, as illustrated in Eq (2). In this study, the resultant field is obtained while substituting the radius of curvature $R = 280$ mm, and the lateral displacement $\Delta x = -0.8$ mm. In this case, both sign and magnitude of the TCs of interfering VBs remain same (such that $l_1 = l_2$).

The simulated phase profile of the VB and its modified copy are shown in Figs 6 (i) and the insets shows the corresponding intensity profiles. It can be observed that the VB produces spiral-shaped interference fringes when interfered with its converging and laterally displaced copy. Because of the spatial shift, singular points of VBs get separated in the plane of interference where spiral and fork-shaped fringes are formed. In these interferograms, the number of spirals (M) is equal to the magnitude of the TC of input VB such that $|l| = M$. The direction of spirals gives the sign of the TC. As shown in Fig 6 (ii), the spirals formed in the fringe patterns have opposite directions for the case of VBs with positive and negative values of TCs. In this case, clockwise direction of the spiral represents positive sign of TC and anticlockwise direction represent negative TC. These analyses can be used for TC measurement, which can be self-verified by the fork-structure that appears simultaneously in the fringe pattern. MZI set-up with a lens can be used to produce these fringe patterns where the lateral shift can be incorporated through the small displacement of mirror used for reflecting the beam.

9.2 Interference with a conjugate replicated beam

In this configuration, the input VB is made to interfere with its copy, which has the same magnitude of TC but its sign is opposite. The interferograms are formed from complete overlapping of beams that improves their quality and allow measurement of high order TCs. The in-line and off-axis interferometric configurations have been discussed in subsequent sub-sections.

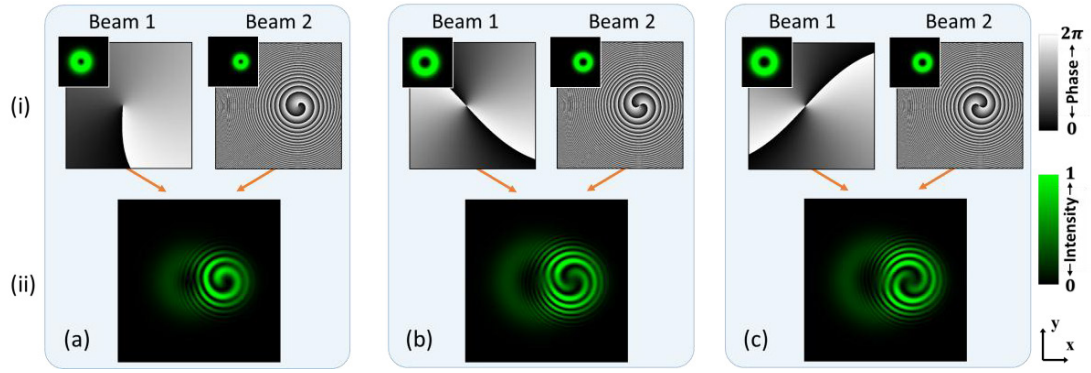

Fig 6. Formation of interferogram consisting of spiral-shaped pattern when VBs interfere with its converging and laterally displaced replicated beam.

(*i*) *In-line interference*

The in-line interference of VBs with exact TCs and curvature creates no fringe pattern and therefore the charge inversion is required [86]. The in-line interference of VBs with its conjugate results into a petal-shaped fringe pattern and when beams have curvature difference, a spiral-shaped fringe pattern is obtained. In this case, the replicated VBs (beam 2) have a different curvature than the input VB, which can be obtained using Eq (4), where the lateral displacement Δx remains zero, the radius of curvature R = 600 mm and the sign of TC is inverted such that $|\, l_2 \,| = -|\, l_1 \,|$. Another interfering beam (beam 1) is given by Eq (2).

Simulated results of the interfering beams and corresponding interferograms are shown in Fig 7. The spiral-shaped structure appears in the fringe pattern at the region of phase singularity. For different TCs, the interfering beams give rise to distinct spiral patterns which can be used for the determination of TC by visual inspection or analysis of the interference pattern. The number of spirals (M) is equal to half the magnitude of TC such that $|l_1| = M/2$ and the sign of TC is indicated by the rotational direction of the spirals. In this case, anticlockwise rotated spirals correspond to the positive value of TC. These fringe patterns have been demonstrated using an MZI set-up [86]. Optical elements such as dove prism or right-angle prism can be used for helicity inversion.

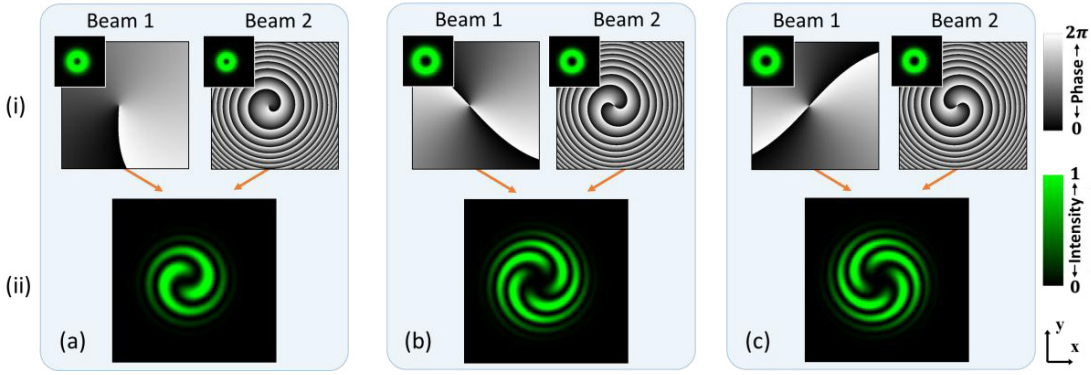

Fig 7. Formation of interferogram consisting of spiral-shaped pattern when VBs interfere with converging replicated beam with inverted helicity.

(*ii*) *Off-axis interference*

This technique requires off-axis interference of input VB with its conjugate copy to obtain the interferogram for TC determination [92]. To ensure that the interfering beams completely overlap each other

in the recording plane, one of them is laterally displaced. Conjugate copy of the input VB is its amplitude split copy with opposite sign of TC. This conjugate copy or in other words, the replicated beam is laterally displaced and tilted before interference which can be represented by Eq (3). In this study, the lateral displacement $\Delta x = -0.22$ mm, tilt angles $\alpha = -0.225$ rad and $\beta = 0$ rad. The helicity of interfering beams is opposite such that $|l_2| = -|l_1|$. The simulated interferogram along with intensity and phase profile of the interfering beams are shown in Fig 8 (i). The null intensity region indicates the presence of singular point and the gradient in the phase profile illustrates the tilt incorporated along the y-direction in the beam 2. In this case, interferograms consist of a fork-shaped fringe pattern. In Fig 8 (ii), the interferogram shown in column (a) corresponds to TC = 1, where fork structures have an extra discontinuous dark fringe (tines) starting from the dislocations.

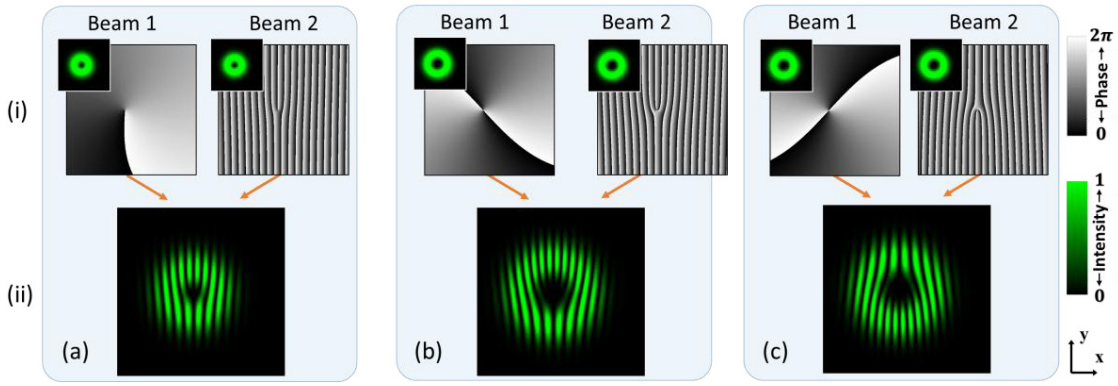

Fig 8. Formation of interferogram consisting of fork-shaped pattern when VBs interfere with the tilted replicated beam with opposite helicity such that the vortices overlap each other.

As the TC value increases, the number of tines of the fork structure (N) also increases which are related to TC as $|l| = (N - 1)/2$. The orientation of a fork structure is used to determine the TC. The fork structure gets inverted for the opposite sign of TC, as shown in Figs 8 (ii-b, c). Formation of these fringe patterns has been demonstrated using MZI where a right angle prism has been used for TC inversion [136]. This approach can be applied to determine the higher values of TC carried by LG beams.

10 Measuring OAM of vector-vortex beams

Scalar-VBs have uniform polarization distribution across the entire beam cross-section. On the other hand, vector-VBs have non-homogeneous polarization distribution and hold both phase as well as polarization singularities [8-9]. These beams have unique properties which are of great interest for various applications such as optical imaging, trapping, and communication [93]. Cylindrical vector beams are a special class of vector beams that have axial symmetry in both amplitude and phase [93]. In addition to phase singularity, such beams hold V-point polarization singularity [8,94]. Cylindrical vector beams when projected on to a Poincaré sphere, span the equator, whereas beams of other class which span the entire surface of the Poincaré sphere is referred to as Full Poincaré beams [7]. Other types of non-uniformly polarized VBs are Bessels-type vector beams and perfect vector-VBs [7,93].

Various methods to measure the OAM carried by vector-VBs have been reported including methods based on diffraction [95], astigmatic transformation [96] and Pancharatnam phase modulation [97]. It has been shown that OAM carried by vector-VBs can be determined by decomposing the beam into its orthogonal polarization components for their TC measurements [98]. Using this approach, techniques of self-referenced interferometry can be also applied to determine the order of vector-VBs. Interferometric techniques can be further utilized to study the properties of other structured light beams such as arbitrarily polarized vector

beams. Such beams use the vectorial nature of light and have potential applications in diverse areas [1,99]. Many new innovations continue to emerge to reduce production and detection of OAM at chip-scale [100].

11 Conclusion and remarks

This paper reviews the development history of OVs and their fundamental properties which led to their widespread applications. Allen *et al* in their book [101] have reprinted many of the papers published during early phases of development of the subject of optical vortices. A review of early work on OVs was also published in 2007 by Singh *et al* [102]. Advances in generation and detection techniques of optical VBs have been discussed. Among various techniques of TC measurement to estimate OAM carried by VBs, the study emphasized on reviewing the progress in self-referenced interferometric techniques. In a comparative study, features of different configurations of self-referenced interferometry and the formation of various interferograms have been discussed. Recent developments show the capability of interferometric techniques in efficiently measuring the OAM of VBs, which have high potential in possible future applications. OV-diagnostics, in general, continues to be a fertile field of investigation as is evident from some representative publications [103-106] in 2020.

References

1. Senthilkumaran P, Singularities in Physics and Engineering, (IOP Publ, UK), 2018.
2. Nye J F, Berry M V, Dislocations in wave trains, *Proc R Soc London A*, 336(1974)165-190.
3. Coullet P, Gil L, Rocca F, Optical vortices, *Opt Commun*, 73(1989)403-408.
4. Vasnetsov M V, Staliunas K, Optical Vortices, (Nova Science Publ), 1999.
5. Kotlyar V V, Kovalev A A, Porfirev A P, Vortex Laser Beams, (CRC Press), 2018.
6. Shen Y, Wang X, Xie Z, Min C, Fu X, Liu Q, Gong M, Yuan X, Optical vortices 30 years on: OAM manipulation from topological charge to multiple singularities, *Light Sci Appl*, 8(2019)90; doi.org/10.1038/s41377-019-0194-2
7. Ruchi, Senthilkumaran P, Pal S K, Phase singularities to polarization singularities, *Int J Opt*, 2020(2020)1-33.
8. Kumar P, Pal S K, Nishchal N K, Senthilkumaran P, Non-interferometric technique to realize vector beams embedded with polarization singularities, *J Opt Soc Am A*, 37(2020)1043-1052.
9. Prati F, Tissoni G, San Miguel M, Abraham N B, Vector vortices and polarization state of low-order transverse modes in a VCSEL, *Opt Commun*, 143(1997)133-146.
10. Gbur G J, Singular Optics, (CRC Press), 2017.
11. Dennis M R, O'Holleran K, Padgett M J, Singular optics: optical vortices and polarization singularities, *Progr Opt*, 53(2009)293-363.
12. Soskin M S, Boriskina S V, Chong Y, Dennis M R, Desyatnikov A, Singular optics and topological photonics, *J Opt*, 19(2017)010401; doi.org/10.1088/2040-8986/19/1/010401.
13. Soskin M S, Gorshkov V N, Vasnetsov M V, Malos J T, Heckenberg N R, Topological charge and angular momentum of light beams carrying optical vortices, *Phys Rev A*, 56(1997)4064-4075.
14. Yao A M, Padgett M J, Orbital angular momentum: origins, behavior and applications, *Adv Opt Photon*, 3(2011)161-204.
15. Arnold S F, Allen L, Padgett M J, Advances in optical angular momentum, *Laser Photon Rev*, 2(2008)299-313.
16. Andrew D L, Babiker M, The Angular Momentum of Light, (Cambridge Univ Press), 2013.
17. Barnett S M, Babiker M, Padgett M J, Optical orbital angular momentum, *Phil Trans R Soc A*, 375(2017)20150444; doi.org/10.1098/rsta.2015.0444.
18. Forbes A, McLaren M, Optical Angular Momentum-The Optics Encyclopedia, (Wiley Publ), 2015.
19. Padgett M J, Orbital angular momentum 25 years on, *Opt Express*, 25(2017)11265-11274.
20. Chen R, Zhou H, Moretti M, Wang X, Li J, Orbital angular momentum waves: generation, detection and emerging applications, IEEE Commun Surv Tutorials, 22(2019)840-868.
21. Ma H, Li X, Zhang H, Tang J, Li H, Tang M, Wang J, Cai Y, Optical vortex shaping via a phase jump factor, *Opt Lett*, 44(2019)1379-1382.

22. Jin L, Li H, Zhao C, Gao W, Generation of Airy vortex beam arrays using computer-generated holography, *J Opt Soc Am A*, 36(2019)1215-1220.
23. O'Holleran K, Padgett M J, Dennis M R, Topology of optical vortex lines formed by the interference of three, four, and five plane waves, *Opt Express*, 14(2006)3039-3044.
24. He H, Friese M E J, Heckenberg N R, Rubinsztein-Dunlop H, Direct observation of transfer of angular momentum to absorptive particles from a laser beam with a phase singularity, *Phys Rev Lett*, 75(1995)826-829.
25. Ritsch-Marte M, Orbital angular momentum light in microscopy, *Phil Trans R Soc*, 375(2017)20150437; doi.org/10.1098/rsta.2015.0437.
26. Singh R K, Senthilkumaran P, Singh K, Focusing of linearly-, and circularly polarized Gaussian background vortex beams by a high numerical aperture system afflicted with third-order astigmatism. *Opt Commun*, 281(2008)5939-5948.
27. Singh R K, Senthilkumaran P, Singh K, Effect of primary coma on the focusing of a Laguerre-Gaussian beam by a high numerical aperture system; vectorial diffraction theory, *J Opt A: Pure Appl Opt*, 10(2008)075008-1-9; doi.org/10.1098/rsta.2015.0437.
28. Torner L, Torres J P, (eds), Twisted Photons: Applications of Light with Orbital Angular Momentum, (Wiley Publ, NY), 2011.
29. Banerji A, Singh R P, Banerjee D, Bandyopadhyay A, Entanglement propagation of a quantum optical vortex state, *Opt Commun*, 380(2016)492-498.
30. Chauhan V S, Kumar R, Manchaiah D, Kumar P, Easwaran R K, Narrowing of electromagnetically induced transparency by using structured coupling light in ^{85} Rb atomic vapor medium, *Laser Phys*, 30(2020)065203; doi.org/10.1088/1555-6611/ab8568.
31. Wang J, Advances in communications using optical vortices, *Photon Res*, 4(2016)B14-B28.
32. Nishchal N K, Optical Cryptosystems, (IOP Publs, Bristol, UK), 2019.
33. Gröblacher S, Jennewein T, Vaziri A, Weihs G, Zeilinger A, Experimental quantum cryptography with qutrits, *New J Phys*, 8(2006)75; doi.org/10.1088/1367-2630/8/5/075.
34. Mirhosseini M, Magaña-Loaiza O S, O'Sullivan M N, Rodenburg B, Malik M, Lavery M P J, Padgett M J, Gauthier D J, Boyd R W, High-dimensional quantum cryptography with twisted light, *New J Phys*, 17(2015)033033; doi.org/10.1088/1367-2630/17/3/033033.
35. Fang X, Ren H, Gu M, Orbital angular momentum holography for high-security encryption, *Nat Photon*, 14(2020)102-108.
36. Ruffato G, Rossi R, Massari M, Mafakheri E, Capaldo P, Romanato F, Design, fabrication and characterization of computer generated holograms for anti-counterfeiting applications using OAM beams as light decoders, *Sci Rep*, 7(2017)18011; doi:https://doi.org/10.1038/s41598-017-18147-7
37. Zhang K, Wang Y, Yuan Y, Burokur S N, A review of orbital angular momentum vortex beams generation: from traditional methods to metasurfaces, *Appl Sci*, 10(2020)1015; doi. org/10.3390/app10031015.
38. Beijersbergen M W, Allen L, van der Veen H E L O, Woerdman J P, Astigmatic laser mode converters and transfer of orbital angular momentum, *Opt Commun*, 96(1993)123-132.
39. Volyar A, Bretsko M, Akimova Y, Egorov Y, Measurement of the vortex and orbital angular momentum spectra with a single cylindrical lens, *Appl Opt*, 58(2019)5748-5755.
40. Vaity P, Singh R P, Topological charge dependent propagation of optical vortices under quadratic phase transformation, *Opt Lett*, 37(2012)1301-1303.
41. Shen D, Zhao D, Measuring the topological charge of optical vortices with a twisting phase, *Opt Lett*, 44(2019)2334-2337.
42. Wang C, Ren Y, Liu T, Luo C, Qiu S, Li Z, Wu H, Generation and measurement of high-order optical vortices by using the cross phase, *Appl Opt*, 59(2020)4040-4049.
43. Reddy S G, Prabhakar S, Aadhi A, Banerji J, Singh R P, Propagation of an arbitrary vortex pair through an astigmatic optical system and determination of its topological charge, *J Opt Soc Am A*, 31(2014)1295-1302.
44. Kotlyar V V, Kovalev A A, Porfirev A P, Astigmatic transforms of an optical vortex for measurement of its topological charge, *Appl Opt*, 56(2017)4095-4103.
45. Lavery M P J, Berkhout G C G, Courtial J, Padgett M J, Measurement of the light orbital angular momentum spectrum using an optical geometric transformation, *J Opt*, 13(2011)064006; doi.org/10.1088/2040-8978/13/6/064006.

46. Wen Y, Chremmos I, Chen Y, Zhu J, Zhang Y, Yu S, Spiral transformation for high-resolution and efficient sorting of optical vortex modes, *Phys Rev Lett*, 120(2018)193904; doi.org/10.1103/PhysRevLett.120.193904.
47. Alperin S N, Niederriter R D, Gopinath J T, Siemens M E, Quantitative measurement of the orbital angular momentum of light with a single, stationary lens, *Opt Lett*, 41(2016)5019-5022.
48. Sahu R, Chaudhary S, Khare K, Bhattacharya M, Wanare H, Jha A K, Angular lens, *Opt Express*, 26(2018)8709-8718.
49. Li C, Zhao S, Efficient separating orbital angular momentum mode with radial varying phase, *Photon Res*, 5(2017)267-270.
50. Mirhosseini M, Malik M, Shi Z, Boyd R W, Efficient separation of the orbital angular momentum eigenstates of light, *Nat Commun*, 4(2013)2781; doi.org/10.1038/ncomms3781.
51. Sztul H I, Alfano R R, Double-slit interference with Laguerre-Gaussian beams, *Opt Lett*, 31(2006)999-1001.
52. de Araujo L E E, Anderson M E, Measuring vortex charge with a triangular aperture, *Opt Lett*, 36(2011)787-789.
53. Liu Y, Sun S, Pu J, Lü B, Propagation of an optical vortex beam through a diamond-shaped aperture, *Opt Laser Technol*, 45(2013)473-479.
54. Ambuj A, Vyas R, Singh S, Diffraction of orbital angular momentum carrying optical beams by a circular aperture, *Opt Lett*, 39(2014)5475-5478.
55. Chen R, Zhang X, Zhou Y, Ming H, Wang A, Zhan Q, Detecting the topological charge of optical vortex beams using a sectorial screen, *Appl Opt*, 56(2017)4868-4872.
56. Guo C S, Lu L L, Wang H T, Characterizing topological charge of optical vortices by using an annular aperture, *Opt Lett*, 34(2009)3686-3688.
57. Zheng S, Wang J, Measuring orbital angular momentum (OAM) states of vortex beams with annular gratings, *Sci Rep*, 7(2017)40781; doi.org/10.1038/srep40781.
58. Prabhakar S, Kumar A, Banerji J, Singh R P, Revealing the order of a vortex through its intensity record, *Opt Lett*, 36(2011)4398-4400.
59. Zhou H, Fu D, Dong J, Zhang P, Chen D, Cai X, Li F, Zhang X, Orbital angular momentum complex spectrum analyzer for vortex light based on the rotational Doppler effect, *Light Sci Appl*, 6(2017)e16251-e16251.
60. Bierdz P, Kwon M, Roncaioli C, Deng H, High fidelity detection of the orbital angular momentum of light by time mapping, *New J Phys*, 15(2013)113062; doi.org/10.1088/1367-2630/15/11/113062.
61. Li S, Zhao P, Feng X, Cui K, Liu F, Zhang W, Huang Y, Measuring the orbital angular momentum spectrum with a single point detector, *Opt Lett*, 43(2018)4607-4610.
62. Zhu J, Zhang P, Fu D, Chen D, Liu R, Zhou Y, Gao H, Li F, Probing the fractional topological charge of a vortex light beam by using dynamic angular double slits, *Photon Res*, 4(2016)187-190.
63. Basistiy I V, Bazhenov V Y, Soskin M S, Vasnetsov M V, Optics of light beams with screw dislocations, *Opt Commun*, 103(1993)422-428.
64. Hu X, Gezhi Z, Sasaki O, Chen Z, Pu J, Topological charge measurement of vortex beams by phase-shifting digital hologram technology, *Appl Opt*, 57(2018)10300-10304.
65. Pan S, Pei C, Liu S, Wei J, Wu D, Liu Z, Yin Y, Xia Y, Yin J, Measuring orbital angular momentums of light based on petal interference patterns, *OSA Continuum*, 1(2018)451-461.
66. Liu G G, Wang K, Lee Y H, Wang D, Li P P, Gou F, Li Y, Tu C, Wu S T, Wang H T, Measurement of the topological charge and index of vortex vector optical fields with a space-variant half-wave plate, *Opt Lett*, 43(2018)823-826.
67. Ma H, Li X, Tai Y, Li H, Wang J, Tang M, Wang Y, Tang J, Nie Z, In-situ measurement of the topological charge of a perfect vortex using the phase shift method, *Opt Lett*, 42(2017)135-138.
68. Gao H, Han Y, Li Y, Zhu D, Sun M, Yu S, Topological charge measurement of concentric OAM states using the phase-shift method, *J Opt Soc Am A*, 35(2018)A40-A44.
69. Berkhout G C G, Beijersbergen M W, Method for probing the orbital angular momentum of optical vortices in electromagnetic waves from astronomical objects, *Phys Rev Lett*, 101(2008)100801; doi.org/10.1103/PhysRevLett.101.100801.
70. Guo C S, Yue S J, Wei G X, Measuring the orbital angular momentum of optical vortices using a multipinhole plate, *Appl Phys Lett*, 94(2009)231104; doi.org/10.1063/1.3151920.

71. Leach J, Courtial J, Skeldon K, Barnett S M, Franke-Arnold S, Padgett M J, Interferometric methods to measure orbital and spin, or the total angular momentum of a single photon, *Phys Rev Lett*, 92(2004)013601;doi.org/10.1103/PhysRevLett.92.013601.
72. Vaughan J M, Willetts D V, Temporal and interference fringe analysis of TEM_{01*} laser modes, *J Opt Soc Am*, 73(1983)1018-1021.
73. White A G, Smith C P, Heckenberg N R, Rubinsztein-Dunlop H, McDuff R, Weiss C O, Tamm C, Interferometric measurements of phase singularities in the output of a visible laser, *J Mod Opt*, 38(1991)2531-2541.
74. Heckenberg N R, McDuff R, Smith C P, White A G, Generation of optical phase singularities by computer-generated holograms, *Opt Lett*, 17(1992)221-223.
75. Kumar P, Nishchal N K, Self-referenced interferometric methods to determine topological charge of vortex beams, Imaging and Applied Optics Congress, OSA Technical Digest, (2020), JTh2A.23; doi.org/10.1364/3D.2020.JTh2A.23
76. Sevryugin A, Gavril'eva K, Shubenkova E, Tursunov I, Touil M, Mermoul A, Venediktov V Y, Comparative study of holographic, interferometric, and other tools for vortex beam analysis, *Proc SPIE*, 10818(2018)108180X; doi.org/10.1117/12.2500490.
77. Chen X, Zhou H, Liu M, Dong J, Measurement of orbital angular momentum by self-interference using a plasmonic metasurface, *IEEE Photon J*, 8(2016)4800308; doi.org/10.1109/JPHOT.2015.2509859.
78. Fedorov E, Gavril'eva K, Gorelaya A, Sevryugin A, Tursunov I, Venediktov D V, Venediktov V Y, Reference beam lacking measurement of topological charge of incoming vortex beam, *Proc SPIE*, 11030(2019)1103002; doi.org/10.1117/12.2521650.
79. Ghai D P, Vyas S, Senthilkumaran P, Sirohi R S, Detection of phase singularity using a lateral shear interferometer, *Opt Lasers Eng*, 46(2008)419-423.
80. Kumar P, Nishchal N K, Self-referenced interference of laterally displaced vortex beams for topological charge determination, *Opt Commun*, 459(2020)125000; doi: org/10.1016/j.optcom.2019.125000.
81. Khajavi B, Galvez E J, Determining topological charge of an optical beam using a wedged optical flat, *Opt Lett*, 42(2017)1516-1519.
82. Lan B, Liu C, Rui D, Chen M, Shen F, Xian H, The topological charge measurement of the vortex beam based on dislocation self-reference interferometry, *Phys Scr*, 94(2019)055502; doi.org/10.1088/1402-4896/ab03a2.
83. Fang Z, Yao Y, Xia K, Li J, Simple Nd:YAG laser generates vector and vortex beam, *Chinese Opt Lett*, 13(2015)031405-031408.
84. Cui S, Xu B, Luo S, Xu H, Cai Z, Luo Z, Pu J, Chávez-Cerda S, Determining topological charge based on an improved Fizeau interferometer, *Opt Express*, 27(2019)12774-12779.
85. Kumar P, Nishchal N K, Self-referenced spiral interferogram using modified lateral shearing Mach-Zehnder interferometer, *Appl Opt*, 58(2019)6827-6833.
86. Harris M, Hill C A, Vaughan J M, Optical helices and spiral interference fringes, *Opt Commun*, 106(1994)161-166.
87. Harris M, Hill C A, Tapster P R, Vaughan J M, Laser modes with helical wave fronts, *Phys Rev A*, 49(1994)3119-3122.
88. Vickers J, Burch M, Vyas R, Singh S, Phase and interference properties of optical vortex beams, *J Opt Soc Am A*, 25(2008)823-827.
89. Li X, Tai Y, Lv F, Nie Z, Measuring the fractional topological charge of LG beams by using interference intensity analysis, *Opt Commun*, 334(2015)235-239.
90. Lv F, Li X, Tai Y, Zhang L, Nie Z, Chen Q, High-order topological charges measurement of LG vortex beams with a modified Mach–Zehnder interferometer, *Optik*, 126(2015)4378-4381.
91. Guo J, Guo B, Fan R, Zhang W, Wang Y, Zhang L, Zhang P, Measuring topological charges of Laguerre–Gaussian vortex beams using two improved Mach–Zehnder interferometers, *Opt Eng*, 55(2016)035104; doi. org/10.1117/1.OE.55.3.035104.
92. Kumar P, Nishchal N K, Modified Mach–Zehnder interferometer for determining the high-order topological charge of Laguerre–Gaussian vortex beams, *J Opt Soc Am A*, 36(2019)1447-1455.
93. Rosales-Guzmán C, Ndagano B, Forbes A, A review of complex vector light fields and their applications, *J Opt*, 20(2018)123001; doi. org/10.1088/2040-8986/aaeb7d.

94. Kumar P, Nishchal N K, Cylindrical vector beams by tailoring single polarization component, Imaging and Applied Optics Congress, OSA Technical Digest, (2020), JTh2A.22;doi.org/10.1364/3D.2020.JTh2A.22.
95. Li Y, Wang X L, Zhao H, Kong L J, Lou K, Gu B, Tu C, Wang H T, Young's two-slit interference of vector light fields, *Opt Lett*, 37(2012)1790-1792.
96. Porfirev A P, Khonina S N, Astigmatic transformation of optical vortex beams with high-order cylindrical polarization, *J Opt Soc Am B*, 36(2019)2193-2201.
97. Zhang D, Feng X, Cui K, Liu F, Huang Y, Identifying orbital angular momentum of vectorial vortices with Pancharatnam phase and Stokes parameters, *Sci Rep*, 5(2015)11982; doi.org/10.1038/srep11982.
98. He Y, Li Y, Fan D, Ye H, Liu J, Xie Z, Wang P, Yang B, Zhou X, Gao Y, Chen S, Effectively identifying the topological charge and polarization order of arbitrary singular light beams based on orthogonal polarization separating, *IEEE Photon J*, 11(2019)1-8.
99. Fatima A, Nishchal N K, Image authentication using a vector beam with sparse phase information, *J Opt Soc Am A*, 35(2018)1053-1062.
100. Hill H M, Chip-scale sensor detects light's orbital angular momentum, *Phys Today*, 73(2020)18-20.
101. Allen L, Barnett S M, Padgett, M J, Orbital Angular Momentum, (IOP, Bristol U K) 2003
102. Singh R K, Senthilkumaran P, Singh K, Laser beams with phase singularities: A review, *Invertis J Sci Technol*, 1(2007)85-124.
103. Alves C R, Amaral J P, Neto A P S, Neto J G M N, Jesus-Silva A J, Measuring the topological charge of coherence vortices through the geometry of the far-field cross-correlation function, *Appl Opt*, 59(2020)153-1557.
104. Bekshaev A, Mikhaylovskaya L, Patil S, Kumar V, Singh R P, Optical-vortex diagnostics via Fraunhofer slit diffraction with controllable wavefront curvature, *J Opt Soc Am A*, 37(2020)760-786.
105. Hosseini-Saber S M A,Akhlagi E A,Saber A, Diffractometry-based vortex beams fractional topological charge-measurement, *Opt Lett*, 45(2020)3478-3481.
106. Hsieh, Y H, Lai, Y H, Hsieh M X, Chen Y F, Characterizing the topological charges distribution of the elliptical beams with vortex lattices, *Opt Lett*, 45(2020)200-204.

[*Received*: 01.09.2020; *accepted*: 07.09.2020]